JEM Journal of Experimental Medicine

BRIEF DEFINITIVE REPORT

Progressive differentiation toward the long-lived plasma cell compartment in the bone marrow

Takuya Koike[1], Kentaro Fujii[2], Kohei Kometani[3], Noah S. Butler[4], Kenji Funakoshi[2], Shinya Yari[5], Junichi Kikuta[5,6,7], Masaru Ishii[5,6,7,8], Tomohiro Kurosaki[2,3,8], and Wataru Ise[1]

The longevity of plasma cells is dependent on their ability to access and reside in so-called niches that are predominantly located in the bone marrow. Here, by employing a traceable method to label recently generated plasma cells, we showed that homeostatic plasma cells in the bone marrow and spleen were continuously replenished by newly generated B220^{hi}MHC-II^{hi} populations that progressively differentiated into B220^{lo}MHC-II^{lo} long-lived plasma cell (LLPC) populations. We also found that, in the bone marrow, germinal center (GC)–independent and GC-dependent plasma cells decayed similarly upon NP-CGG engagement, and both entered the B220^{lo}MHC-II^{lo} LLPC pool. Compared with NP^{+}B220^{hi}MHC-II^{hi} plasma cells, NP^{+}B220^{lo}MHC-II^{lo} cells were more immobilized in the bone marrow niches and showed better survival potential. Thus, our results suggest that the adhesion status of bone marrow plasma cells is dynamically altered during their differentiation and is associated with provision of survival signals.

Introduction

Antibodies (Abs) are produced by terminally differentiated plasma cells (PCs) and have distinct functions depending on their isotype. While the majority of PCs generated during an immune response die within days after their formation (termed short-lived PCs [SLPCs]), a small minority persists for months, years, or even decades (Nutt et al., 2015). These long-lived PCs (LLPCs) are found in locations distinct from their site of generation, often in the bone marrow (BM). Hence, the notion has developed that longevity of PCs in the BM and elsewhere depends on them accessing specialized microenvironments called survival niches (Lindquist et al., 2019). Given that the half-life of circulating Abs is a few days to weeks, the maintenance of pathogen- or self-antigen-specific PCs is essential for achieving durable immune protection or pathology. Therefore, dissecting and defining the events underlying the generation and maintenance of LLPCs are critical for understanding how Ab-mediated immunity is maintained.

In regard to generation of LLPCs, it is widely thought that LLPCs emanate mainly from germinal centers (GCs) in response to T cell–dependent (TD) antigens (Chan and Brink, 2012; Good-Jacobson and Shlomchik, 2010). This model is mainly supported by studies showing that the majority of BM PCs generated in response to TD antigens harbor high-affinity and class-switched Abs (Smith et al., 1997). Considering that GC-independent PCs are generated earlier than GC-dependent PCs during an immune response, these observations may support the idea that newly generated PCs occupy niches by replacing the pre-existing LLPCs (Radbruch et al., 2006). This concept, however, has been recently challenged by two lines of evidence. First, long-lived Ab production was also described in T cell–independent antigen responses, which do not elicit GC reactions (Bortnick et al., 2012; Taillardet et al., 2009; Foote et al., 2012). Second, following TD antigen immunization, BM LLPCs were still generated even when the GC response was blocked experimentally (Bortnick et al., 2012). Although these experiments are informative, caution is required to interpret them. Contemporary studies detect the numbers of PCs residing in the BM and considered them as LLPCs; however, this population also includes the recently generated SLPCs residing in the BM (Chernova et al., 2014). Given the evidence that GCs are maintained for a relatively longer time, for instance 2 or 3 mo, than previously expected (Cirelli et al., 2019), the PCs in the BM might still

[1]Regulation of Host Defense Team, Division of Microbiology and Immunology, Center for Infectious Disease Education and Research, Osaka University, Osaka, Japan; [2]Laboratory of Lymphocyte Differentiation, WPI Immunology Frontier Research Center, Osaka University, Osaka, Japan; [3]Laboratory for Lymphocyte Differentiation, RIKEN Center for Integrative Medical Sciences, Kanagawa, Japan; [4]Department of Microbiology and Immunology, The University of Iowa, Iowa City, IA, USA; [5]Department of Immunology and Cell Biology, Graduate School of Medicine and Frontier Biosciences, Osaka University, Osaka, Japan; [6]Laboratory of Immunology and Cell Biology, WPI Immunology Frontier Research Center, Osaka University, Osaka, Japan; [7]Laboratory of Bioimaging and Drug Discovery, National Institutes of Biomedical Innovation, Health and Nutrition, Osaka, Japan; [8]Division of Microbiology and Immunology, Center for Infectious Disease Education and Research, Osaka University, Osaka, Japan.

Correspondence to Tomohiro Kurosaki: kurosaki@ifrec.osaka-u.ac.jp; Wataru Ise: wise@ifrec.osaka-u.ac.jp.

include SLPCs even 2 mo after immunization. Hence, it is unclear whether or not GC reactions indeed affect the generation and survival of LLPCs in the BM.

Here, to overcome the limitation of the current assay system, we employed a time-stamping method for PCs, thereby allowing us to directly measure the decay of the labeled BM PCs in a wild-type setting. Using this method, we first demonstrated that the homeostatic PC pool in the BM and spleen (SPL) was continuously replenished by recently arriving B220^{hi}MHC-II^{hi} cells, small fraction of which then differentiated into a B220^{lo}MHC-II^{lo} LLPC pool. Second, in the 4-hydroxy-3-nitrophenylacetyl–chicken γ-globulin (NP-CGG) immune response, we could not find significant survival differences between GC-independent and -dependent NP^{+} PCs in the BM. Finally, in contrast to NP^{+}B220^{hi}MHC-II^{hi} PCs in the BM, the NP^{+}B220^{lo}MHC-II^{lo} LLPCs with greater survival potential were more immobilized to the niches, suggesting an association between adhesion strength and provision of survival signals to PCs.

Results and discussion

Establishment of a PC fate mapping system

To track long-term survival of PCs, we sought to generate an experimental system that could irreversibly label PCs in an inducible manner. To this end, we established a new mouse line in which the sequence encoding a tamoxifen-inducible Cre recombinase-estrogen receptor 2 fusion protein (creER^{T2}) was inserted downstream of the *Prdm1* (*Blimp1*) promoter (Fig. S1 A). The mice were crossed with Ai14 mice (Madisen et al., 2010), in which a transgene encoding the red fluorescent protein variant tdTomato with a loxP-franked stop cassette is under control of the *Rosa26* promoter (Fig. S1 A). In the "Blimp1-creER^{T2} × Ai14" mice, only cells expressing *Blimp1* at the time of tamoxifen treatment should express tdTomato. Indeed, when tamoxifen was administered to unimmunized Blimp1-creER^{T2} × Ai14 mice, CD138^{hi}TACI^{hi} PCs in SPL and BM were efficiently labeled with tdTomato, while CD138^{-}B220^{+} cells remained unlabeled (Fig. S1 B). Among B cell–lineage cells, only PCs in BM or SPL were labeled after tamoxifen treatment (Fig. S1 C). *Blimp1* has been shown to be expressed not only in PCs, but in a fraction of effector T cells and myeloid cells (Nadeau and Martins, 2021). Consistently, tdTomato^{+} cells mostly consist of PCs, but also include CD4^{+} T cells and macrophages (Fig. S1, D and E), suggesting that this system faithfully reports Blimp-1 expression in vivo.

Homeostatic turnover of PC populations in distinct tissues

In our system, PCs generated de novo after tamoxifen treatment are not labeled, therefore allowing us to track the fate of PCs that existed at given time points. To monitor long-term survival of PCs in the steady state, tamoxifen was administered to naive Blimp1-creERT2 × Ai14 mice for three consecutive days and the survival of tdTomato + PCs in SPL, BM, and gut lamina propria (LP) was followed over a year (Fig. 1 A). PCs in BM or SPL are IgM^{+}, IgA^{+}, or IgG^{+}, whereas those in LP are mostly IgA^{+}. After tamoxifen treatment, most of the PCs in each tissue were efficiently labeled with tdTomato. However, the frequency of tdTomato^{+} PCs, irrespective of isotypes or tissues, dropped to <60% in 28 d, and was as few as 3–20% at a year after (Fig. 1, B–D, left graphs). Enumeration of tdTomato^{+} PCs revealed the half-life of PCs in SPL or BM that was comparable with that reported recently using a similar fate mapping system (Xu et al., 2020; Fig. S2 A). We also found that the half-life of PCs varies depending on isotypes. IgG^{+} PCs decayed faster than IgM^{+} or IgA^{+} PCs did in 6 mo (Fig. S2 B). 30% of IgA^{+} or 24% of IgG^{+} PCs in BM survived over a year, whereas IgM^{+} PCs showed better survival (Fig. 1 B, right graphs). These results suggest that the homeostatic PC pool is dynamically regulated by continuous influx of newly generated PCs and loss of pre-existing PCs in BM, SPL, and LP, the latter probably mediated by cell death in situ and/or exit from the tissues. Nevertheless, some fractions of pre-existing PCs are still maintained over a year in these tissues (Fig. 1, B–D, right graph), suggesting the existence of subpopulations of LLPCs. Comparison of each tissue indicated that half-life of PCs in BM is longer than that of PCs in SPL or LP (Fig. S2) and that BM maintained more PCs after 1 yr, irrespective of isotypes (Fig. 1, B–D, right graph). These results suggest that BM niches are superior to those in other tissues.

Identification of B220^{lo}MHC-II^{lo} LLPCs

Based on the above findings, we next sought to identify the subpopulations containing LLPCs in BM and SPL and, if present, determine how such a population is stable during homeostatic turnover. It has been shown that there is considerable heterogeneity in the human BM PC population and that LLPCs are contained in the CD19^{-}CD38^{hi}CD138^{+} population (Halliley et al., 2015). However, this human study, because of the lack of synchronous traceable experimental systems, did not clarify two possibilities in regard to generation mechanism of LLPCs in BM. First, after arriving at BM, a short-lived population is progressively differentiated to LLPCs during their BM residence (progressive differentiation model). Second, before arriving at, two distinct precursors (SLPC and LLPC precursors) are already generated, which would activate specific differentiation, homing, and/or survival programs that eventually determine their survival upon residence in BM (pre-determined model). To distinguish these possibilities, we decided to utilize CD138-DTR Tg mice, in which CD138^{+} cells can be depleted by administrating diphtheria toxin (DT; Vijay et al., 2020). Because CD138 is expressed not only in PCs but also in non-hematopoietic compartments, such as endothelial cells (Zhang et al., 2021), DT induction is lethal to CD138-DTR Tg mice (data not shown). To avoid this lethality, we generated CD138-DTR × Blimp1-creERT2 × Ai14 BM chimeric mice. Importantly, this system depletes PCs at the time of DT treatment but allows development of homeostatic PCs thereafter (Fig. S3, A–C). Hence, after depletion of pre-existing PCs, we could label de novo–generated PCs and trace their phenotype and survival (Fig. 2 A). We focused on the expression of B220 and MHC class-II (MHC-II) because these markers have been shown to be downregulated during PC generation and maturation (Tellier et al., 2016). We found that the majority of PCs that appeared in BM immediately after DT and tamoxifen treatment consisted of B220^{hi}MHC-II^{hi} double positive (DP) cells (Fig. 2 B). At day 28, DP cells were substantially decreased and instead, B220^{lo}MHC-II^{hi} single positive (SP)

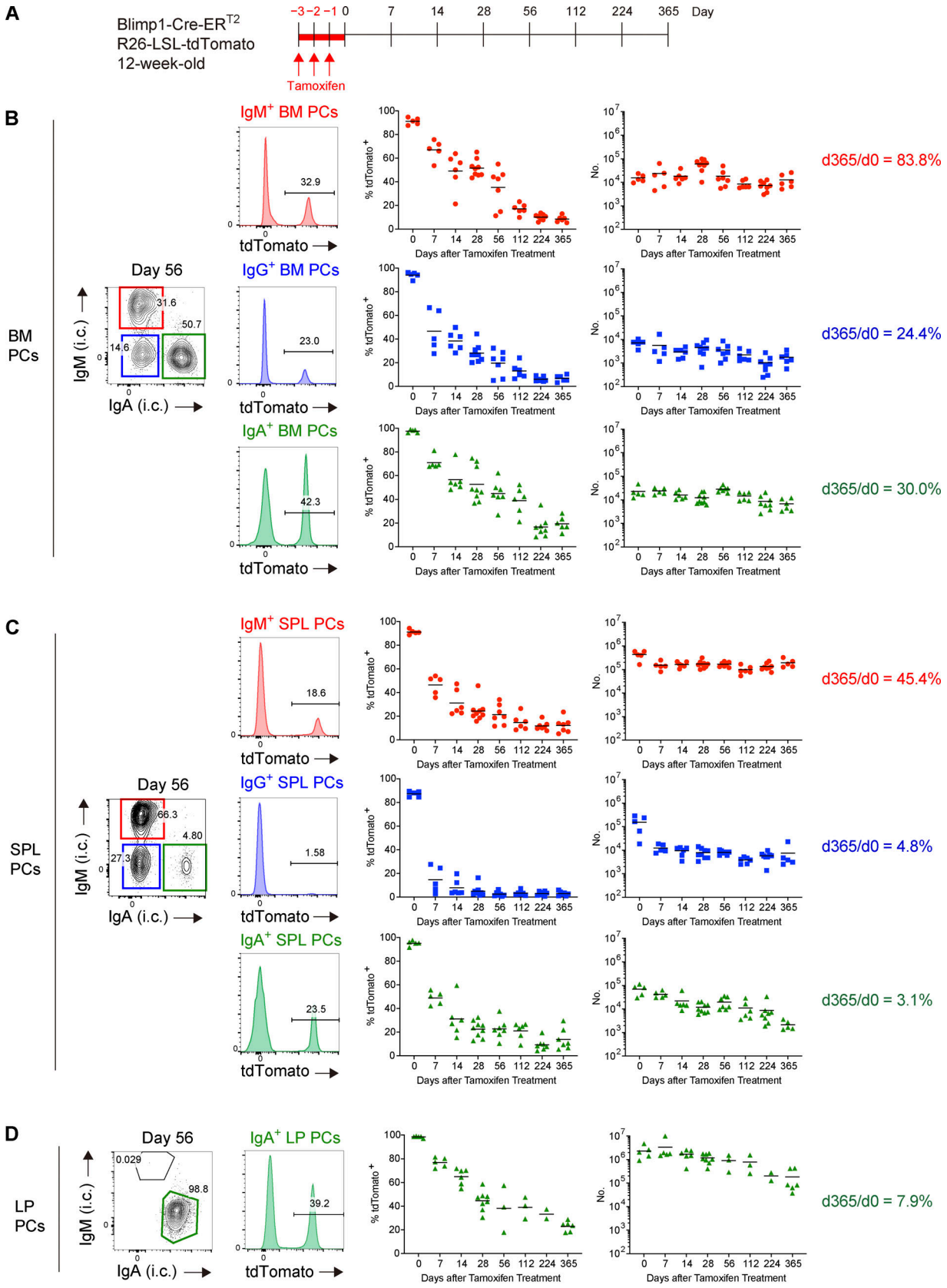

Figure 1. **Homeostatic PC turnover in BM, SPL, and LP. (A–D)** Blimp1-Cre-ER^{T2} R26-LSL-tdTomato mice were treated with tamoxifen for 3 d. At the indicated time points after tamoxifen treatment, PCs in each organ were analyzed by FCM. The details of the mice and the experimental system are shown in Fig. S1. **(A)** Schematic of the experimental procedure. **(B–D)** Intracellular (i.c.) IgM or IgA expression (contour plots), tdTomato expression (histograms) by PCs of each isotype at day 56 after tamoxifen treatment (IgG$^+$ PCs were defined as IgG$^+$/IgM$^-$/IgA$^-$). The right two columns show the frequency and the absolute

numbers of tdTomato+ cells for PCs of each isotype at the indicated time points in BM (B), SPL (C), and LP (D). Five to nine mice for PCs in BM or SPL or two to eight mice for PCs in LP were analyzed at each time point. Data collected from 14 independent experiments are combined in the right two columns.

cells and B220^{lo}MHC-II^{lo} double negative (DN) cells emerged. At a later time point (84 d), DN cells became the major population among surviving BM PCs and, importantly, the absolute number of DN cells remained constant. A similar transition was also observed in SPL (Fig. 2 C).

Next, we characterized the cell cycle status of PC subpopulations in BM or SPL using mVenus-p27K^{-} (Oki et al., 2014) or Fucci-mAGmKO2 mice (Sakaue-Sawano et al., 2008) to monitor G0 or S/G2/M phases, respectively (Fig. 2 D). In both SPL and BM, a substantial fraction of DP cells was in the S/G2/M phase, whereas most DN cells were in G0. We then examined the survival potential of each PC subpopulation by culturing them in vitro (Fig. 2 E). As previously reported (Rozanski et al., 2011; Rozanski et al., 2015), most of PCs were viable at least for a day

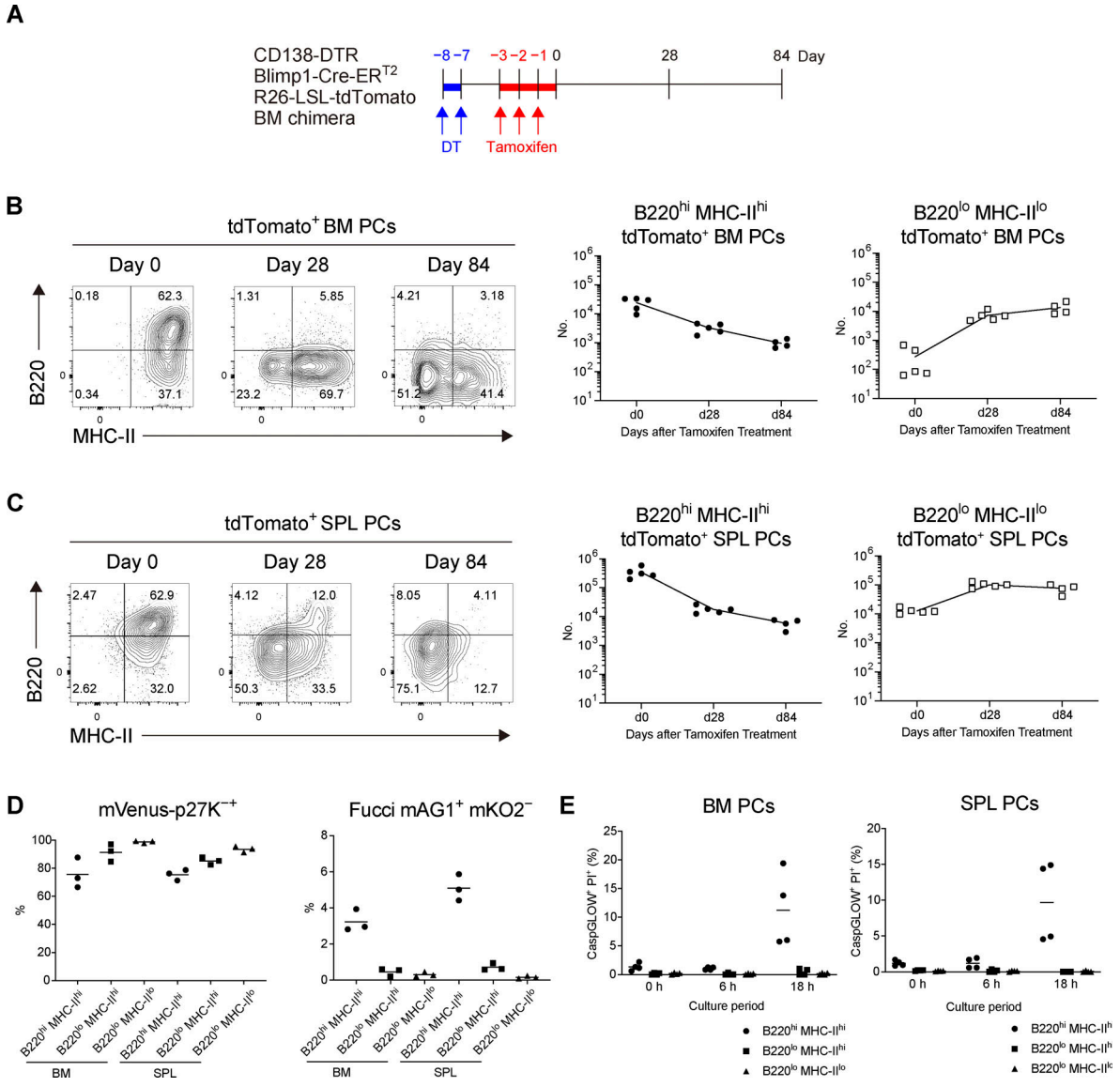

Figure 2. **Differentiation of B220^{lo}MHC-II^{lo} PCs from B220^{hi}MHC-II^{hi} PCs. (A and B)** BM chimeric mice were generated by transfer of BM cells from CD138-DTR Blimp1-CreER^{T2} R26-LSL-tdTomato mice into x-ray irradiated mice. In the chimeric mice, pre-existing PCs derived from donor BM cells were depleted by DT treatment (Fig. S3, A–C), and de novo–generated PCs from the same BM cell origin were subsequently labeled by tamoxifen administration. These tdTomato+ PCs were analyzed by FCM at the indicated time points. **(A)** Schematic of the experimental procedure. **(B and C)** The expression of B220 and MHC-II on tdTomato+ PCs and the absolute numbers of B220^{hi}MHC-II^{hi} and B220^{lo}MHC-II^{lo} tdTomato+ PCs in BM (B) and SPL (C) at the indicated time points after tamoxifen treatment. Four or five mice were analyzed at the indicated time points. **(D)** Cell cycle status of each PC subset from SPL or BM analyzed by using mVenus-p27K- mice (left, G0) and Fucci mice (right, S, G2, M). Three mice each were analyzed. **(E)** The frequency of late apoptotic (CaspGLOW+ PI+) cells in each PC subset after in vitro culture for the indicated times. PCs isolated from four mice were analyzed. Data are representative of two independent experiments.

in vitro. After 18 h of culture, a significant number of DP cells underwent apoptosis (CaspGLOW$^+$/PI$^+$), whereas the DN cells did not show any sign of cell death. These analyses further support our conclusion that DP and DN cells are SLPCs and LLPCs, respectively, the latter of which exit cell cycle and acquire enhanced survival potential during progressive differentiation. Together, these results suggest that the progressive differentiation model is likely taking place, although we could not completely exclude the possibility that B220^{hi}MHC-II^{hi} populations are composed of two subpopulations (SLPC- and LLPC-precursor-derived PCs).

We further wished to confirm that the DN population contains LLPCs by examining long-term survival of homeostatic BM or splenic PCs in wild-type Blimp1-creER^{T2} × Ai14 mice (Fig. 3). Immediately after tamoxifen treatment, we observed three cell populations, DP, SP, and DN cells, among IgM$^+$, IgG$^+$, or IgA$^+$ BM PC (Fig. 3 A). The frequency of DP cells quickly decreased and, conversely, that of DN cells increased over time. The majority of BM IgM$^+$, IgG$^+$, and IgA$^+$ cells were DN cells at 1 yr after labeling. Of note, enumeration of DP and DN PCs demonstrated that DP cells are short-lived, whereas DN cells are long-lived, with barely any decay (Fig. 3 A and Fig. S2 C). Indeed, 85% of DN IgM$^+$, 91% of DN IgG$^+$, and 65% of DN IgA$^+$ PCs persisted over 1 yr, indicating that LLPCs are contained in the DN population in BM. In SPL, similar kinetics were observed; however, half-life of DN cells in SPL was shorter than that of DN cells in BM (Fig. S2 C) and only 6% of DN IgA$^+$ PCs persisted after 1 yr (Fig. 3 B). The above detailed survival curves of DP and DN PCs indicated that the better survival of overall IgM$^+$ PCs shown in Fig. 1 could be majorly due to less decrease of DP PCs. Considering that the isotype-specific heavy chain is able to transmit the signal, at least to some extent (Engels et al., 2009), together with the evidence that IgM$^+$ and IgA$^+$, but not IgG$^+$, PCs do still express B cell receptor on the cell surface (Pinto et al., 2013), these isotype-specific signals might involve in survival of DN PCs. Alternatively, like seen in survival of IgA$^+$ memory B cells (Wang et al., 2012), transcription factors differentially expressed in IgM$^+$, IgG$^+$, or IgA$^+$ PCs (Higgins et al., 2022) may participate in their longevity.

Survival of GC-independent or GC-derived PCs in BM

In terms of generation of LLPCs by vaccination or infection, one widely accepted model is that LLPCs preferentially emanate from the GC reaction (Good-Jacobson and Shlomchik, 2010; Chan and Brink, 2012). This is based on the observation that the majority of antigen-specific PCs in BM harbor somatically mutated and high-affinity antibodies (Smith et al., 1997). Several recent studies have argued against this notion, by demonstrating the existence of long-lived antibody responses in the absence of a GC response (Bortnick et al., 2012; Bortnick and Allman, 2013). However, longevity of PCs that are generated independently of the GC (pre-GC) or derived from the GC (post-GC) has never been directly tested in a wild-type setting. Thus, by utilizing the S1pr2-creER^{T2} GC–B cell fate mapping reporter mice (Shinnakasu et al., 2016) and immunization with NP-CGG, we sought to determine whether GC experience is required for PCs to participate in the long-lived compartment in BM. At day 7 after immunization, the NP-specific PC pool was entirely occupied by pre-GC PCs (Fig. 4 A). The frequency of post-GC PCs increased progressively, and they became dominant in the NP-specific PC pool at day 56 (Fig. 4 A and Fig. S3 D), which was expected from previous studies (Weisel et al., 2016). The continuous influx of post-GC PCs into the BM due to a sustained GC response might underestimate the survival ability of pre-GC PCs. Thus, we next terminated an ongoing GC reaction by anti-CD40L mAb treatment and examined the survival of pre-GC and post-GC PCs in a competitive setting (Fig. 4 B). At day 14 after immunization, pre-GC and post-GC PCs existed almost equally in the NP-specific PC pool (Fig. 4 B). In sharp contrast to the previous experiment (Fig. 4 A), the ratio of pre-GC and post-GC PCs was stable over time (Fig. 4 B), suggesting that the cell intrinsic ability to survive in BM is similar between pre-GC and post-GC PCs.

We further examined long-term survival of pre-GC or post-GC PCs in BM, by specifically labeling and chasing each type of PC. In order to chase pre-GC PCs, NP-specific B1-8^{germ} B cells harboring Blimp1-creER^{T2} reporter were transferred and labeled at earlier time points when GCs were not yet formed (Fig. 4 C). For tracing post-GC PCs, B1-8^{germ} B cells expressing S1pr2-creER^{T2} reporter were transferred and labeled, followed by anti-CD40L treatment to prevent influx of PCs from later in the GC response (Fig. 4 D). As shown in Fig. 4, C and D, pre-GC and post-GC PCs decayed in a similar manner. 10–20% of both pre- and post-GC PCs could survive in the BM for at least 2 mo. For both types of PCs, recently arrived cells were uniformly B220^{hi}MHC-II^{hi}, which then disappeared within a month (Fig. 4, C and D, and Fig. S3 E). B220^{lo}MHC-II^{lo} cells concomitantly emerged during this period and survived (Fig. 4, C and D, and Fig. S3 E), suggesting that these two types of PCs follow the same maturation process as observed in homeostatic PCs. Taken together, our results indicate that both pre-GC and post-GC PCs can enter the B220^{lo}MHC-II^{lo} long-lived compartment.

Regarding how newly generated PCs are allowed to survive in the BM, two mutually exclusive models exist, in which the capacity of the BM niche is assumed to be unlimited or saturable (Radbruch et al., 2006; Wilmore and Allman, 2017). In the latter model, newly formed PCs must compete for limited survival niches and supplant the pre-exiting PCs to achieve long-term survival. Our data rather favor the former model in which newly generated PCs occupy a vacant BM niche. First, decay of pre-GC and latecomer post-GC PCs did not differ in survival in the BM. Second, we noticed that, in homeostatic PCs, absolute numbers of PCs in BM and SPL gradually increased along with aging (Fig. S1 F), thereby supporting the notion that the survival niche is not saturated. The seeming disparity between our data and previous idea is probably due to the following reason. GCs are reported to continue for a long time (for instance, 2 or 3 mo; Cirelli et al., 2019) and to produce PCs at a temporally late phase (Weisel et al., 2016). Assuming that these PCs constantly accumulate as LLPCs in the BM during immune responses, these mutated PCs are probably over-represented at a late time point.

Maturation-dependent PC dynamics in the BM niche

Previous studies have demonstrated that PCs in BM physically contact with reticular stromal cells (Tokoyoda et al., 2004),

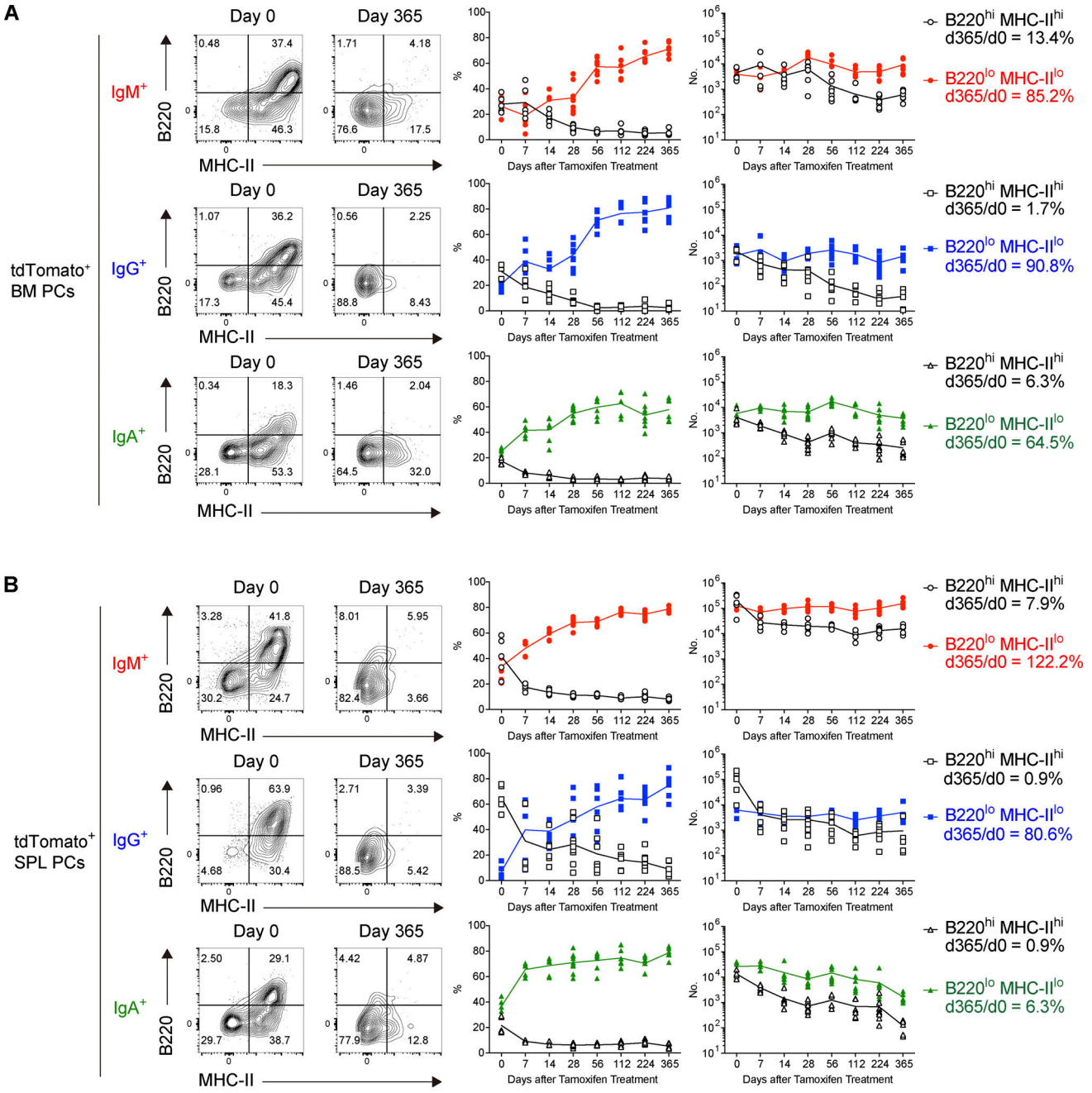

Figure 3. **Identification of B220^{lo}MHC-II^{lo} long-lived PCs. (A and B)** The frequencies of B220^{hi}MHC-II^{hi} and B220^{lo}MHC-II^{lo} tdTomato^{+} PCs of each isotype, and their absolute numbers in BM (A) and SPL (B) at the indicated time points using the same experimental procedure as shown in Fig. 1. Five to nine mice were analyzed at each time point. Data collected from 14 independent experiments are combined.

eosinophils, dendritic cells, or megakaryocytes (Zehentmeier et al., 2014). The interaction between PCs and these other cells is thought to be essential for PCs to receive survival signals. However, it has been unclear whether PC dynamics in the BM environment are changed depending on their maturation status or longevity. To address this issue, we performed intravital imaging of antigen-specific BM PCs that were derived from B1-8^{germ} Blimp1-creER^{T2} reporter B cells (Fig. 5 A and Video 1). At day 12 after immunization, antigen-specific PCs, most of which were at B220^{hi}MHC-II^{hi} DP stage, were motile and migratory in BM with significant velocity (Fig. 5, B–D). In sharp contrast, PCs at day 54 were sessile and immobilized in the BM environment (Fig. 5, B–D). These observations suggest that PC behavior in BM is dynamically altered during their differentiation to B220^{lo}MHC-II^{lo} DN LLPCs and that strength or stability of contact with the BM niche might be associated with PC longevity.

Based on the niche model, it is critical to understand the mechanisms by which PCs access the niches, for instance in the BM, and the extent to which variation in PC survival is due to niches, PCs, or a combination of both factors (Robinson et al.,

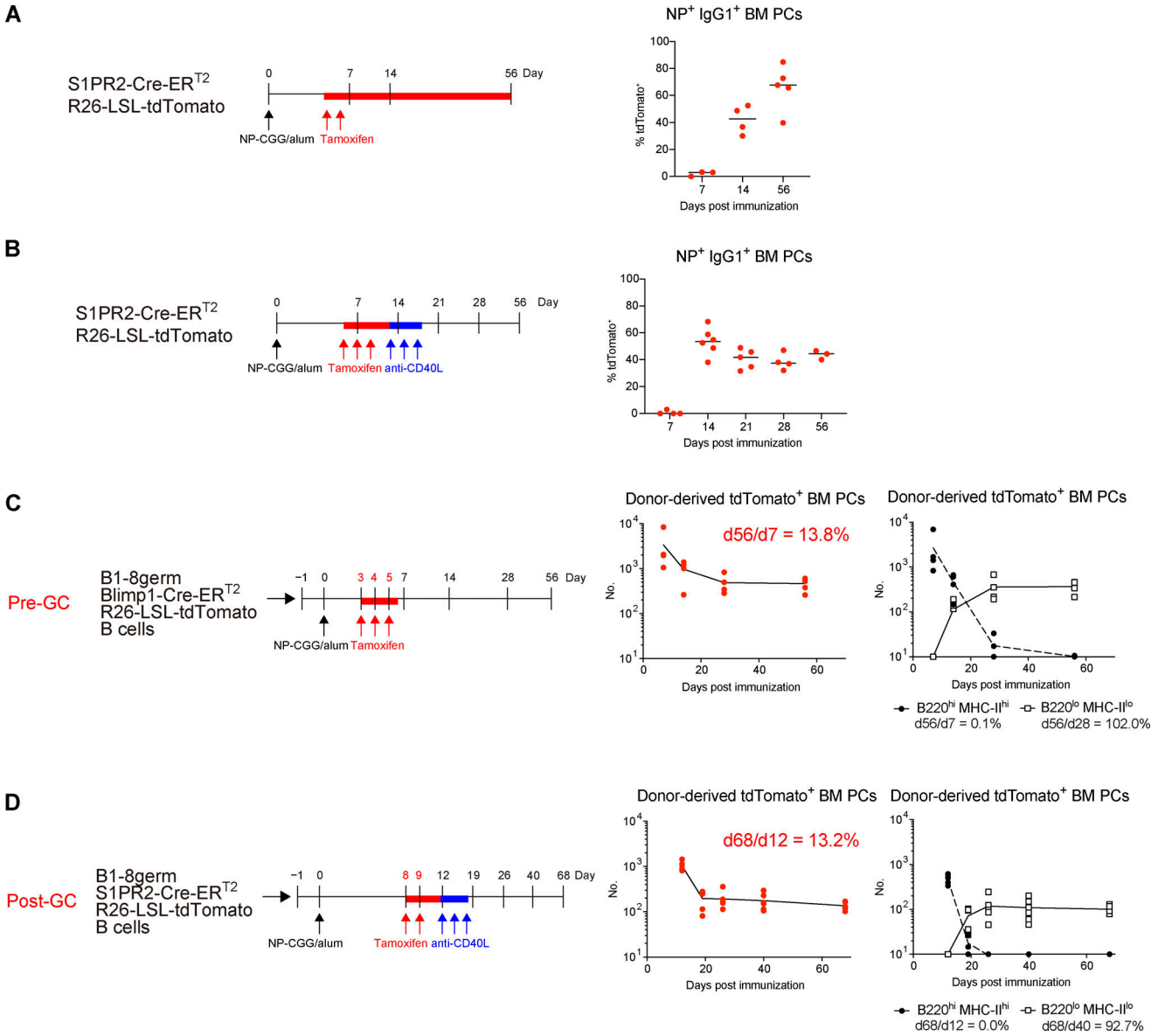

Figure 4. **Survival of GC-independent and GC-derived PCs. (A)** S1PR2-CreER^{T2} R26-LSL-tdTomato mice were immunized with NP-CGG in alum and then treated with tamoxifen on days 5 and 6. The frequency of tdTomato$^+$ cells among NP$^+$ IgG1$^+$ BM PCs at the indicated time points is shown. Four or five mice were analyzed at the indicated time points. **(B)** S1PR2-CreER^{T2} R26-LSL-tdTomato mice were immunized with NP-CGG in alum and then treated with tamoxifen on days 6, 7, and 8. On days 13, 15, and 17 after immunization, GCs were depleted by anti-CD40L treatment. The frequency of tdTomato$^+$ cells among NP$^+$ IgG1$^+$ BM PCs at the indicated time points is shown. Three to six mice were analyzed at each time point. **(C)** B6 mice were transferred with splenic B cells from B1-8^{germ} Blimp1-CreER^{T2} R26-LSL-tdTomato mice, immunized with NP-CGG in alum, and then treated with tamoxifen from day 3 to 5 after immunization. At the indicated time points after immunization, absolute numbers of donor-derived tdTomato$^+$ PCs (left) and B220^{hi}MHC-II^{hi} and B220^{lo}MHC-II^{lo} PC subsets (right) in BM were analyzed. Four or five mice were analyzed at each time point. **(D)** B6 mice were transferred with splenic B cells from B1-8^{germ} S1PR2-CreER^{T2} R26-LSL-tdTomato mice, immunized with NP-CGG in alum and then treated with tamoxifen at days 8 and 9 after immunization. For GC depletion, the mice were injected i.p. with anti-CD40L mAb at days 12, 14, and 16 after immunization. At the indicated time points after immunization, absolute numbers of donor-derived tdTomato$^+$ BM PCs (left) and B220^{hi}MHC-II^{hi} and B220^{lo}MHC-II^{lo} PC subsets (right) in BM were analyzed. Five or six mice were analyzed at each time point. All data are representative of two independent experiments except B, where data from two independent experiments are combined. The gating strategy for NP-specific PCs is shown in Fig. S3, D and E.

2020). Here, as a first step toward these goals, we traced how PCs newly arrived at the niche-containing tissues differentiate into the LLPC pool under homeostatic and protein immunization conditions. In both cases, we demonstrate that a progressive differentiation process takes place in which changes from B220^{hi}MHC-II^{hi} to B220^{lo}MHC-II^{lo} subsets reflect the longevity of the cells. In our NP-specific PC case, 10–20% of B220^{hi}MHC-II^{hi} PCs differentiate into B220^{lo}MHC-II^{lo} pool (Fig. 4, C and D). In addition, we demonstrate that in homeostatic conditions, continuous replenishment of PCs occurs in niche-containing tissues, suggesting that the gradual increase in the total number of BM PCs over mouse ages (Fig. S1 F) is probably due to

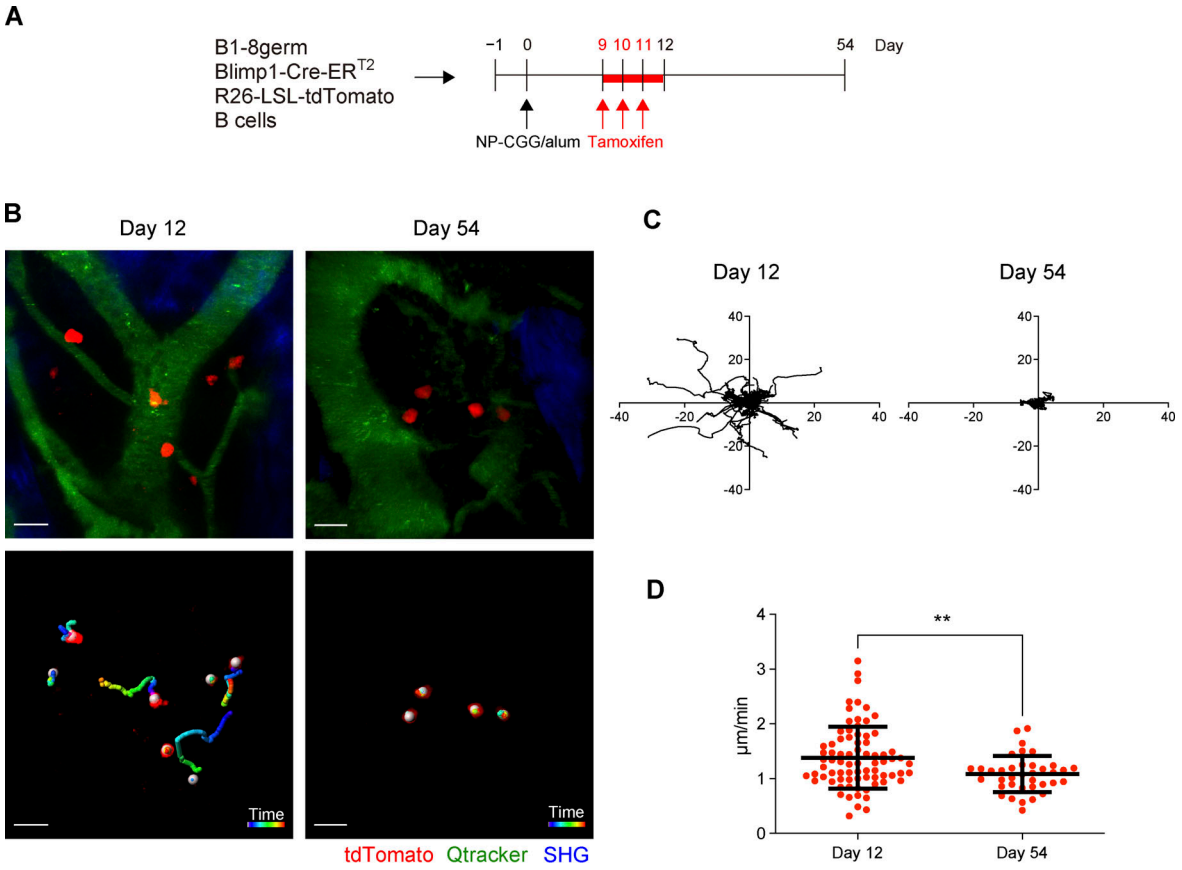

Figure 5. **Maturation-dependent PC dynamics in the BM niche.** B6 mice were transferred with splenic B cells from B1-8^{germ} Blimp1-CreER^{T2} R26-LSL-tdTomato mice, immunized with NP-CGG in alum, and then treated with tamoxifen from day 9 to 11 after immunization. Intravital BM imaging was performed using these mice on day 12 and 54 after immunization. **(A)** Schematic of the experimental procedure. **(B)** A representative maximum-intensity projection image of skull bone tissues from the mice at the indicated time points after immunization (top). Red, PCs expressing tdTomato; green, blood vessels (Qdot); blue, bone tissues (SHG). Scale bar, 20 μm. Trajectory of these PCs measured for 1 h (bottom). White spheres were automatically generated by Imaris software recognizing tdTomato$^+$ cells. **(C)** Displacement of PCs in the x–y plane during 1 h of observation in the mice at the indicated time points after immunization. **(D)** Mean track speed of PCs at the indicated time points. Data are pooled from two mice with 77 cells and three mice with 37 cells at day 12 and 54 after immunization, respectively. All data are pooled from two independent experiments. **P < 0.01 by two-tailed unpaired Student's *T* test. The imaging data are available in Video 1.

continuous excess of such replenishment over cell death in these tissues along with mouse aging.

Benet et al. have recently reported that BM PCs are motile (Benet et al., 2021). Because they analyzed the behavior of homeostatic PCs in unimmunized mice and did not distinguish LLPCs from SLPCs, most of PCs that were motile and migratory could have been SLPCs. Nonetheless, they found that the integrin VLA4 promoted PC arrest in the BM. It has been demonstrated that BM PCs express VLA4 as well as LFA-1 and that functional blockade of these molecules purges these cells from BM niches, which resulted in a decreased antigen-specific serum Ab titer (DiLillo et al., 2008). Thus, mobilization differences in SLPCs and LLPCs shown here suggest the possibility that VLA4/LFA-1–mediated adhesion is dynamically regulated during the differentiation to LLPCs and is critical for LLPC development and durable Ab responses.

Although our data clearly indicate that LLPC emanate from B220^{hi}MHC-II^{hi} DP population, it is still unclear whether all DP cells have the same potential to become LLPC and their fate is stochastically determined, or only a fraction of DP cells have such potential to become LLPC. Clarification of this issue would be important for understanding the reason why the duration of Ab production varies widely across vaccines (Bhattacharya, 2022; Amanna et al., 2007).

Materials and methods

Mice

C57BL/6JJcl mice were purchased from CLEA Japan. All of the following mice were backcrossed to B6 or congenic B6 CD45.1$^+$ mouse strains: B1-8^{germ} (Shinnakasu et al., 2016), Blimp1-CreER^{T2}, S1pr2-CreER^{T2} (Shinnakasu et al., 2016), R26-LSL-tdTomato (Ai14; Madisen et al., 2010), CD138-DTR (Vijay et al., 2020), Fucci (Sakaue-Sawano et al., 2008), and mVenus-p27K$^-$ (Oki et al., 2014). To generate Blimp1-CreER^{T2} mice, Cre-ER^{T2} cassette was knocked-in downstream of the start codon of *Blimp1* gene (Fig. S1 A). 8–12-wk-old mice were used for all experiments. In Figs. 2, 4, C and D, and 5, only male mice were used. In Figs. 1, 3, and 4, A and B, roughly equal number of male and female mice was mixed and used. All mice were bred and

maintained under specific pathogen–free conditions, and all animal experiments were performed under the institutional guidelines of Osaka University.

Immunization, treatments, and adoptive transfer

Mice were immunized i.p. with 30 µg of NP-CGG in alum (Inoue et al., 2021). To induce the deletion of the loxP-flanked STOP cassette by Cre-mediated recombination, 2 mg tamoxifen (Sigma-Aldrich) in sunflower seed oil (Sigma-Aldrich) was orally administered to mice once per day for 2 or 3 d. For GC depletion, the mice were injected i.p. with 250–300 µg of anti-CD40L (Bio X Cell; BE0017-1) every other day for 1 wk. For PC depletion, CD138-DTR BM chimeric mice were injected i.p. with 250 ng of DT (Millipore) for 2 d. B cells were purified from SPL by magnetic cell depletion using AutoMACS system (Miltenyi Biotech) with Streptavidin MicroBeads (Miltenyi Biotech) and biotinylated mAbs against CD43 (13-0431-82; Invitrogen), CD4 (13-0042-86; eBioscience), CD8α (13-0081-86; Invitrogen), CD11b (13-0112-86; eBioscience), Gr-1 (13-5931-86; eBioscience), NK1.1 (13-5941-85; Invitrogen), and Ter119 (Ter119; Invitrogen). The frequency of NP^+ cells in B cells was determined by flow cytometry (FCM). The naive B cells containing 2.5×10^4 NP^+ B cells per mouse were transferred into B6 mice, which were then immunized i.p. with NP-CGG in alum on the next day.

FCM and cell sorting

For all the FCM analyses, single-cell suspensions from SPL, BM (tibia and femur), and LP were depleted of RBCs by RBC lysis buffer (Thermo Fisher Scientific), blocked with anti-CD16/32 (2.4G2; BD Bioscience), and then stained with the following mAbs for 30 min at 4°C in PBS supplemented with 0.5% BSA, 2 mM EDTA: from BD Biosciences, CD138 (740880), CD19 (553784), IgG1 (553441, 553443), IgG3 (553403), MHC-II (742894), and TACI (742840); from Bio Rad, IgG2c (STAR135F); from Biolegend, B220 (103204, 103222), CD115 (130059), CD11c (117322), Gr-1 (108423), NK1.1 (108706), and Streptavidin (405229, 563858); from eBioscience, CD3ε (48-0031-82); from Invitrogen, B220 (56-0452-82), CD11c (11-0114-82), CD3ε (13-0031-82), CD45.1 (17-0453-82), F4/80 (69-4801-80), MHC-II (17-5321-82, 11-5321-82), NK1.1 (13-5941-85), Streptavidin (47-4317-82), and Ter119 (13-5921-85); from R&D systems, DT receptor (DTR; hHB-EGF). Stained cells were analyzed using FACSymphony A3, FACSAriaII, FACSCantoII (BD Biosciences), or Attune NxT (Thermo Fisher Scientific) instruments. The data were analyzed using Flowjo (Tree Star). Dead cells, detected using propidium iodide or Fixable Viability Dye (eBioscience), were gated out in all FCM experiments. To avoid the quenching of tdTomato after cell fixation and permeabilization, intracellular staining was performed as follows: In the first step, surface Ag-stained cells washed with PBS were fixed by Fixation Buffer (BD Biosciences) for 30 min at 4°C. After washing with PBS, the second step using Fixation and Permeabilization Buffer (BD Biosciences) for 30 min at 4°C allows the intracellular staining Abs to enter the cell while preserving the fluorescence of tdTomato. Subsequent washing step and intracellular staining for Ig and NP were performed using Perm/Wash buffer (BD Biosciences). For the intracellular staining of Ig in homeostatic PCs, samples were stained with Abs against IgM (47-5790-82; Invitrogen), IgA (407004; Biolegend), and IgG (IgG1: 553443; BD Biosciences, IgG2b: 406706; Biolegend, IgG2c: STAR135F; Bio Rad, and IgG3: 553403; BD Biosciences) for 30 min at room temperature. NP-binding Ig was detected with NP_{14}-BSA-Alexa Fluor 647 (Haniuda et al., 2016). For the staining of LP cells, the cells were first fixed and permeabilized with Foxp3/Transcription Factor Staining Buffer Set (Invitrogen) and were then stained with anti-IRF4 (48-9858-80; Invitrogen) and anti-Blimp1 (150004; Biolegend) over night at 4°C, followed by staining with Abs against Ig for 30 min at room temperature. LP PCs were defined as $IRF4^+Blimp1^+$ cells.

Isolation of LP leukocytes from small intestine

Isolation of LP leukocytes from small intestine was performed based on previous report (Moro et al., 2015). Peyer's Patches, mesentery, and feces were removed from small intestine. The remaining intestine were opened longitudinally, washed with PBS to deplete feces and mucus, and cut into 1-cm pieces. To remove epithelial cells and intraepithelial lymphocytes, these pieces were stirred in PBS containing 1 mM EDTA for 20 min at 37°C. Intestinal pieces were vigorously washed with PBS and then minced into 1–2-mm pieces. The mince was stirred two times in 0.5 mg/ml collagenase D (Roche) and 50 µg/ml DNase I (Roche) for 30 min at 37°C. LP lymphocytes were separated from the digested suspension by collecting at the interface between 40 and 80% discontinuous Percoll gradient (Cytiva).

Apoptosis assay

PCs were enriched from splenocytes or BM cells using AutoMACS system with biotinylated anti-CD138 (142512; Biolegend) and Streptavidin MicroBeads. 2×10^5 enriched cells were resuspended in 200 µl complete medium (RPMI-1640 medium [Wako] supplemented with 10% heat-inactivated fetal bovine serum, 1 mM sodium pyruvate, 50 µM 2-mercaptoethanol, 10 mM Hepes, pH 7.5, 100 U/ml penicillin, and 100 µg/ml streptomycin), and then cultured at 37°C in 5% CO_2 for 0, 6, and 18 h. Cultured cells were immediately mixed with FITC-VAD-FMK (CaspGlow; BioVision) and incubated for 30 min at 37°C. Subsequently, these cells were stained with Abs and propidium iodide, and then analyzed by FCM.

Intravital two-photon BM imaging

All surgery and subsequent microscope observation were performed on mice subjected to isoflurane inhalation anesthesia. Handling of mice for intravital two-photon BM imaging was performed as described previously (Furuya et al., 2018). Briefly, parietal bones were exposed by the incision of skin, and then the head holder was attached to parietal bones. After the head holder was fixed to the stage, BM cavities in parietal bones were observed using two-photon excitation microscopy. For the staining of blood vessels, 100–200 nmol of Qtracker 655 Vascular Labels (Thermo Fisher Scientific) was administered from tail vein.

The imaging system consisted of a Nikon upright two-photon microscope (A1R-MP) equipped with an ×25 water-immersion objective (APO, N.A. 1.1; Nikon). The system was driven by a femtosecond-pulsed infrared laser (Chameleon Vision II Ti:

Sapphire; Coherent, Inc.). Using a Nikon upright microscope, multi-fluorescent images were acquired by direct detection of fluorescence using four external non-descanned detectors equipped with dichroics and emission filters including an infrared-cut filter (DM685), three dichroic mirrors (DM495, DM560, and DM607), and four emission filters (492/SP for the second harmonic generation [SHG] image, 525/50 for autofluorescence, 583/22 for tdTomato, 675/67 for Qtracker 655). The excitation wavelength was 940 nm. For intravital time-lapse imaging, 12 sequential image stacks were acquired at 3-µm vertical steps with ×1.5 zoom, 512 × 512 x–y resolution, and time resolution of 30 s. Using NIS Elements integrated software (Nikon), drift was corrected in these sequential images and the autofluorescence of these images was eliminated by spectral unmixing. Using Imaris software (Bitplane), color intensity in these images was adjusted, and then TIFF files were exported. Some consecutive TIFF files were converted to movie using After Effects (Adobe). Track speed mean and displacement in the XY plane were analyzed by the tracking tool of Imaris software.

Quantification and statistical analysis

Statistical analysis was performed with a two-tailed unpaired Student's *t*-test using Graphpad Prism software. P values <0.05 were considered significant (**P < 0.01). The curve-fit and half-life calculations were done using Graphpad Prism software, as previously described (Xu et al., 2020).

Online supplemental material

Fig. S1 shows the experimental system that was used for PC labeling and fate mapping (related to Fig. 1). Fig. S2 shows the calculated half-life of PC population in BM, SPL, or LP (related to Figs. 1 and 3). Fig. S3 shows the gating strategy for identifying de novo generating homeostatic PCs from CD138-DTR cells or NP-specific PCs induced by immunization (related to Figs. 2 and 4). Video 1 shows the dynamic behavior of antigen-specific PCs in BM (related to Fig. 5).

Acknowledgments

We thank Dr. Toshihiko Oki and Dr. Toshio Kitamura (The Institute of Medical Science, The University of Tokyo, Tokyo, Japan) for mVenus-p27K⁻ transgenic mice; Dr. David Tarlinton for sharing unpublished data; Dr. Saori Fukao and Dr. Yoshihito Nihei for isolation of LP lymphocytes; and Ms. Nozomi Shimada and Ms. Rie Yamawaki for technical assistance.

This work was supported by Nippon Foundation (to W. Ise), Otsuka Pharmaceutical Co., Ltd. (to T. Kurosaki), Grand-in-Aid for JSPS Fellows (JP22J00313 to T. Koike), Grand-in-Aid for Young Scientists (JP20K16283 to T. Koike), Japan Society for the Promotion of Science KAKENHI (JP22H00450 to T. Kurosaki, JP18KK0227 and JP20H03503 to W. Ise), the SENSHIN Medical Research Foundation (to T. Koike), the Uehara Memorial Foundation (to W. Ise), the Naito Foundation (to W. Ise), and Daiichi Sankyo Foundation of Life Science (to W. Ise).

Author contributions: T. Kurosaki and W. Ise conceptualized research; T. Koike, K. Fujii, and K. Funakoshi performed the experiments; K. Kometani and N.S. Butler provided resources; S. Yari, J. Kikuta, and M. Ishii performed intravital imaging analysis; T. Kurosaki and W. Ise supervised the research; and T. Koike, T. Kurosaki, and W. Ise wrote the manuscript.

Disclosures: The authors declare no competing interests exist.

Submitted: 7 October 2022
Revised: 7 November 2022
Accepted: 23 November 2022

References

Amanna, I.J., N.E. Carlson, and M.K. Slifka. 2007. Duration of humoral immunity to common viral and vaccine antigens. *N. Engl. J. Med.* 357: 1903–1915. https://doi.org/10.1056/NEJMoa066092

Benet, Z., Z. Jing, and D.R. Fooksman. 2021. Plasma cell dynamics in the bone marrow niche. *Cell Rep.* 34:108733. https://doi.org/10.1016/j.celrep.2021.108733

Bhattacharya, D. 2022. Instructing durable humoral immunity for COVID-19 and other vaccinable diseases. *Immunity*. 55:945–964. https://doi.org/10.1016/j.immuni.2022.05.004

Bortnick, A., and D. Allman. 2013. What is and what should always have been: Long-lived plasma cells induced by T cell-independent antigens. *J. Immunol.* 190:5913–5918. https://doi.org/10.4049/jimmunol.1300161

Bortnick, A., I. Chernova, W.J. Quinn III, M. Mugnier, M.P. Cancro, and D. Allman. 2012. Long-lived bone marrow plasma cells are induced early in response to T cell-independent or T cell-dependent antigens. *J. Immunol.* 188:5389–5396. https://doi.org/10.4049/jimmunol.1102808

Chan, T.D., and R. Brink. 2012. Affinity-based selection and the germinal center response. *Immunol. Rev.* 247:11–23. https://doi.org/10.1111/j.1600-065X.2012.01118.x

Chernova, I., D.D. Jones, J.R. Wilmore, A. Bortnick, M. Yucel, U. Hershberg, and D. Allman. 2014. Lasting antibody responses are mediated by a combination of newly formed and established bone marrow plasma cells drawn from clonally distinct precursors. *J. Immunol.* 193:4971–4979. https://doi.org/10.4049/jimmunol.1401264

Cirelli, K.M., D.G. Carnathan, B. Nogal, J.T. Martin, O.L. Rodriguez, A.A. Upadhyay, C.A. Enemuo, E.H. Gebru, Y. Choe, F. Viviano, et al. 2019. Slow delivery immunization enhances HIV neutralizing antibody and germinal center responses via modulation of immunodominance. *Cell.* 177:1153–1171.e28. https://doi.org/10.1016/j.cell.2019.04.012

DiLillo, D.J., Y. Hamaguchi, Y. Ueda, K. Yang, J. Uchida, K.M. Haas, G. Kelsoe, and T.F. Tedder. 2008. Maintenance of long-lived plasma cells and serological memory despite mature and memory B cell depletion during CD20 immunotherapy in mice. *J. Immunol.* 180:361–371. https://doi.org/10.4049/jimmunol.180.1.361

Engels, N., L.M. König, C. Heemann, J. Lutz, T. Tsubata, S. Griep, V. Schrader, and J. Wienands. 2009. Recruitment of the cytoplasmic adaptor Grb2 to surface IgG and IgE provides antigen receptor-intrinsic costimulation to class-switched B cells. *Nat. Immunol.* 10:1018–1025. https://doi.org/10.1038/ni.1764

Foote, J.B., T.I. Mahmoud, A.M. Vale, and J.F. Kearney. 2012. Long-term maintenance of polysaccharide-specific antibodies by IgM-secreting cells. *J. Immunol.* 188:57–67. https://doi.org/10.4049/jimmunol.1100783

Furuya, M., J. Kikuta, S. Fujimori, S. Seno, H. Maeda, M. Shirazaki, M. Uenaka, H. Mizuno, Y. Iwamoto, A. Morimoto, et al. 2018. Direct cell-cell contact between mature osteoblasts and osteoclasts dynamically controls their functions in vivo. *Nat. Commun.* 9:300. https://doi.org/10.1038/s41467-017-02541-w

Good-Jacobson, K.L., and M.J. Shlomchik. 2010. Plasticity and heterogeneity in the generation of memory B cells and long-lived plasma cells: The influence of germinal center interactions and dynamics. *J. Immunol.* 185: 3117–3125. https://doi.org/10.4049/jimmunol.1001155

Halliley, J.L., C.M. Tipton, J. Liesveld, A.F. Rosenberg, J. Darce, I.V. Gregoretti, L. Popova, D. Kaminiski, C.F. Fucile, I. Albizua, et al. 2015. Long-lived plasma cells are contained within the CD19(-)CD38(hi)CD138(+) subset in human bone marrow. *Immunity*. 43:132–145. https://doi.org/10.1016/j.immuni.2015.06.016

Haniuda, K., S. Fukao, T. Kodama, H. Hasegawa, and D. Kitamura. 2016. Autonomous membrane IgE signaling prevents IgE-memory formation. *Nat. Immunol.* 17:1109–1117. https://doi.org/10.1038/ni.3508

Higgins, B.W., A.G. Shuparski, K.B. Miller, A.M. Robinson, L.J. McHeyzer-Williams, and M.G. McHeyzer-Williams. 2022. Isotype-specific plasma cells express divergent transcriptional programs. *Proc. Natl. Acad. Sci. USA*. 119:e2121260119. https://doi.org/10.1073/pnas.2121260119

Inoue, T., R. Shinnakasu, C. Kawai, W. Ise, E. Kawakami, N. Sax, T. Oki, T. Kitamura, K. Yamashita, H. Fukuyama, and T. Kurosaki. 2021. Exit from germinal center to become quiescent memory B cells depends on metabolic reprograming and provision of a survival signal. *J. Exp. Med.* 218:e20200866. https://doi.org/10.1084/jem.20200866

Lindquist, R.L., R.A. Niesner, and A.E. Hauser. 2019. In the right place, at the right time: Spatiotemporal conditions determining plasma cell survival and function. *Front. Immunol.* 10:788. https://doi.org/10.3389/fimmu.2019.00788

Madisen, L., T.A. Zwingman, S.M. Sunkin, S.W. Oh, H.A. Zariwala, H. Gu, L.L. Ng, R.D. Palmiter, M.J. Hawrylycz, A.R. Jones, et al. 2010. A robust and high-throughput Cre reporting and characterization system for the whole mouse brain. *Nat. Neurosci.* 13:133–140. https://doi.org/10.1038/nn.2467

Moro, K., K.N. Ealey, H. Kabata, and S. Koyasu. 2015. Isolation and analysis of group 2 innate lymphoid cells in mice. *Nat. Protoc.* 10:792–806. https://doi.org/10.1038/nprot.2015.047

Nadeau, S., and G.A. Martins. 2022. Conserved and unique functions of Blimp1 in immune cells. *Front. Immunol.* 12:805260. https://doi.org/10.3389/fimmu.2021.805260

Nutt, S.L., P.D. Hodgkin, D.M. Tarlinton, and L.M. Corcoran. 2015. The generation of antibody-secreting plasma cells. *Nat. Rev. Immunol.* 15:160–171. https://doi.org/10.1038/nri3795

Oki, T., K. Nishimura, J. Kitaura, K. Togami, A. Maehara, K. Izawa, A. Sakaue-Sawano, A. Niida, S. Miyano, H. Aburatani, et al. 2014. A novel cell-cycle-indicator, mVenus-p27K-, identifies quiescent cells and visualizes G0-G1 transition. *Sci. Rep.* 4:4012. https://doi.org/10.1038/srep04012

Pinto, D., E. Montani, M. Bolli, G. Garavaglia, F. Sallusto, A. Lanzavecchia, and D. Jarrossay. 2013. A functional BCR in human IgA and IgM plasma cells. *Blood*. 121:4110–4114. https://doi.org/10.1182/blood-2012-09-459289

Radbruch, A., G. Muehlinghaus, E.O. Luger, A. Inamine, K.G.C. Smith, T. Dörner, and F. Hiepe. 2006. Competence and competition: The challenge of becoming a long-lived plasma cell. *Nat. Rev. Immunol.* 6:741–750. https://doi.org/10.1038/nri1886

Robinson, M.J., R.H. Webster, and D.M. Tarlinton. 2020. How intrinsic and extrinsic regulators of plasma cell survival might intersect for durable humoral immunity. *Immunol. Rev.* 296:87–103. https://doi.org/10.1111/imr.12895

Rozanski, C.H., R. Arens, L.M. Carlson, J. Nair, L.H. Boise, A.A. Chanan-Khan, S.P. Schoenberger, and K.P. Lee. 2011. Sustained antibody responses depend on CD28 function in bone marrow-resident plasma cells. *J. Exp. Med.* 208:1435–1446. https://doi.org/10.1084/jem.20110040

Rozanski, C.H., A. Utley, L.M. Carlson, M.R. Farren, M. Murray, L.M. Russell, J.R. Nair, Z. Yang, W. Brady, L.A. Garrett-Sinha, et al. 2015. CD28 promotes plasma cell survival, sustained antibody responses, and BLIMP-1 upregulation through its distal PYAP proline motif. *J. Immunol.* 194:4717–4728. https://doi.org/10.4049/jimmunol.1402260

Sakaue-Sawano, A., H. Kurokawa, T. Morimura, A. Hanyu, H. Hama, H. Osawa, S. Kashiwagi, K. Fukami, T. Miyata, H. Miyoshi, et al. 2008. Visualizing spatiotemporal dynamics of multicellular cell-cycle progression. *Cell*. 132:487–498. https://doi.org/10.1016/j.cell.2007.12.033

Shinnakasu, R., T. Inoue, K. Kometani, S. Moriyama, Y. Adachi, M. Nakayama, Y. Takahashi, H. Fukuyama, T. Okada, and T. Kurosaki. 2016. Regulated selection of germinal-center cells into the memory B cell compartment. *Nat. Immunol.* 17:861–869. https://doi.org/10.1038/ni.3460

Smith, K.G., A. Light, G.J. Nossal, and D.M. Tarlinton. 1997. The extent of affinity maturation differs between the memory and antibody-forming cell compartments in the primary immune response. *EMBO J.* 16:2996–3006. https://doi.org/10.1093/emboj/16.11.2996

Taillardet, M., G. Haffar, P. Mondière, M.-J. Asensio, H. Gheit, N. Burdin, T. Defrance, and L. Genestier. 2009. The thymus-independent immunity conferred by a pneumococcal polysaccharide is mediated by long-lived plasma cells. *Blood*. 114:4432–4440. https://doi.org/10.1182/blood-2009-01-200014

Tellier, J., W. Shi, M. Minnich, Y. Liao, S. Crawford, G.K. Smyth, A. Kallies, M. Busslinger, and S.L. Nutt. 2016. Blimp-1 controls plasma cell function through the regulation of immunoglobulin secretion and the unfolded protein response. *Nat. Immunol.* 17:323–330. https://doi.org/10.1038/ni.3348

Tokoyoda, K., T. Egawa, T. Sugiyama, B.-I. Choi, and T. Nagasawa. 2004. Cellular niches controlling B lymphocyte behavior within bone marrow during development. *Immunity*. 20:707–718. https://doi.org/10.1016/j.immuni.2004.05.001

Vijay, R., J.J. Guthmiller, A.J. Sturtz, F.A. Surette, K.J. Rogers, R.R. Sompallae, F. Li, R.L. Pope, J.-A. Chan, F. de Labastida Rivera, et al. 2020. Infection-induced plasmablasts are a nutrient sink that impairs humoral immunity to malaria. *Nat. Immunol.* 21:790–801. https://doi.org/10.1038/s41590-020-0678-5

Wang, N.S., L.J. McHeyzer-Williams, S.L. Okitsu, T.P. Burris, S.L. Reiner, and M.G. McHeyzer-Williams. 2012. Divergent transcriptional programming of class-specific B cell memory by T-bet and RORα. *Nat. Immunol.* 13:604–611. https://doi.org/10.1038/ni.2294

Weisel, F.J., G.V. Zuccarino-Catania, M. Chikina, and M.J. Shlomchik. 2016. A temporal switch in the germinal center determines differential output of memory B and plasma cells. *Immunity*. 44:116–130. https://doi.org/10.1016/j.immuni.2015.12.004

Wilmore, J.R., and D. Allman. 2017. Here, there, and anywhere? Arguments for and against the physical plasma cell survival niche. *J. Immunol.* 199:839–845. https://doi.org/10.4049/jimmunol.1700461

Xu, A.Q., R.R. Barbosa, and D.P. Calado. 2020. Genetic timestamping of plasma cells in vivo reveals tissue-specific homeostatic population turnover. *eLife*. 9:e59850. https://doi.org/10.7554/eLife.59850

Zehentmeier, S., K. Roth, Z. Cseresnyes, Ö. Sercan, K. Horn, R.A. Niesner, H.-D. Chang, A. Radbruch, and A.E. Hauser. 2014. Static and dynamic components synergize to form a stable survival niche for bone marrow plasma cells. *Eur. J. Immunol.* 44:2306–2317. https://doi.org/10.1002/eji.201344313

Zhang, D., L. Li, Y. Chen, J. Ma, Y. Yang, S. Aodeng, Q. Cui, K. Wen, M. Xiao, J. Xie, et al. 2021. Syndecan-1, an indicator of endothelial glycocalyx degradation, predicts outcome of patients admitted to an ICU with COVID-19. *Mol. Med.* 27:151. https://doi.org/10.1186/s10020-021-00412-1

Supplemental material

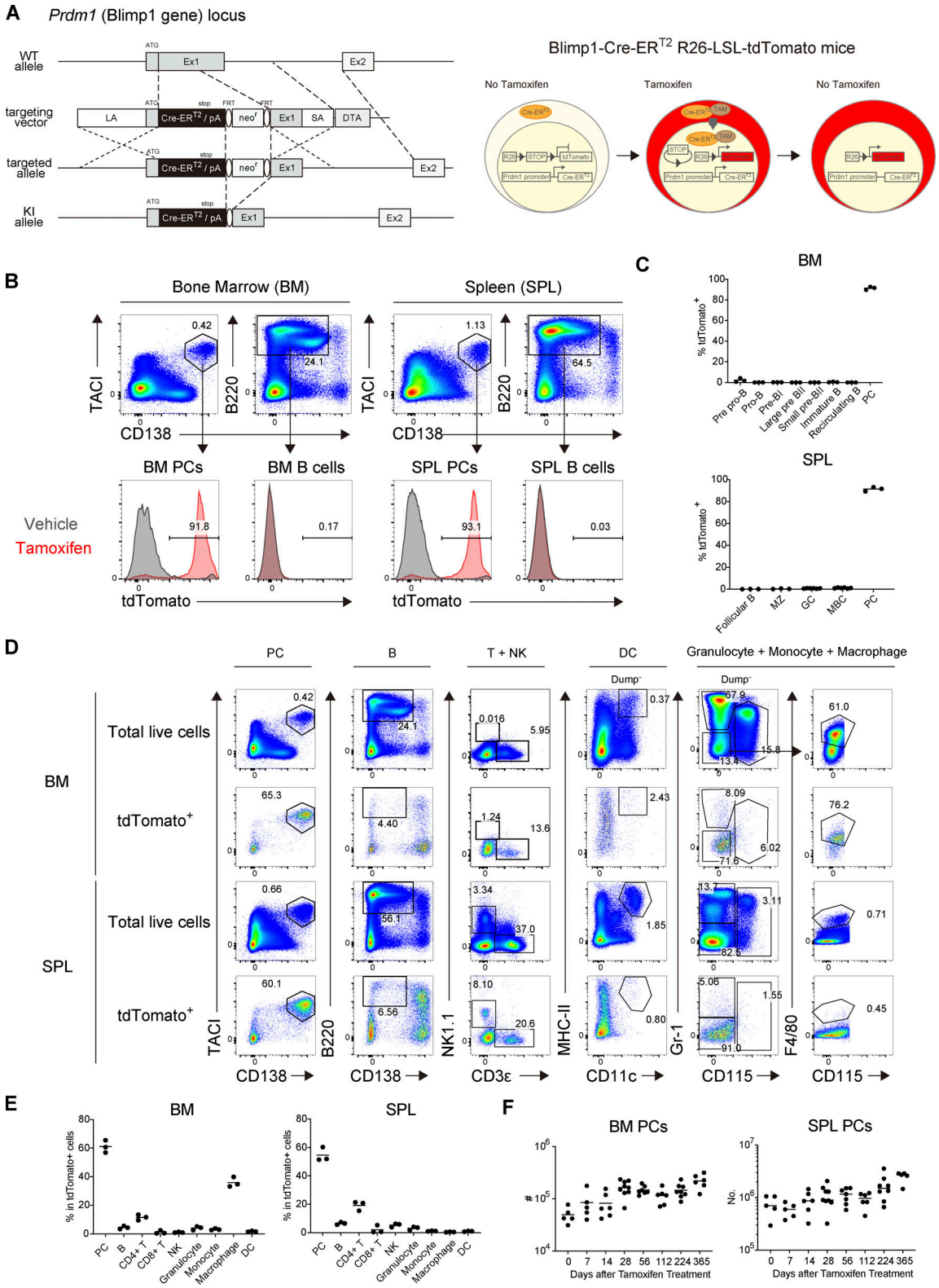

Figure S1. **Establishment of the PC fate mapping system. (A)** Schematic representation of the generation of Blimp1-CreER^{T2} knock-in mice (left) and the PC-linage tracing system using Blimp1-CreER^{T2} R26-LSL-tdTomato mice (right). **(B and C)** Blimp1-CreER^{T2} R26-LSL-tdTomato mice were treated with tamoxifen for 3 d. **(B)** The expression of tdTomato in PCs (CD138$^+$ TACI$^+$) or B cells (B220$^+$ CD138$^-$) in SPL or BM. Data are representative of three independent experiments. **(C)** The frequency of tdTomato$^+$ cells in B cells or PCs in SPL and BM after tamoxifen treatment of Blimp1-CreER^{T2} R26-LSL-tdTomato mice. Three mice each were analyzed. **(D and E)** The frequency of each immune cell type expressing tdTomato. Three mice were analyzed. Data are representative of two independent experiments. **(F)** Absolute numbers of total BM PCs and SPL PCs analyzed in Fig. 1. Five to seven mice were analyzed at each time point. Data collected from 14 independent experiments are combined.

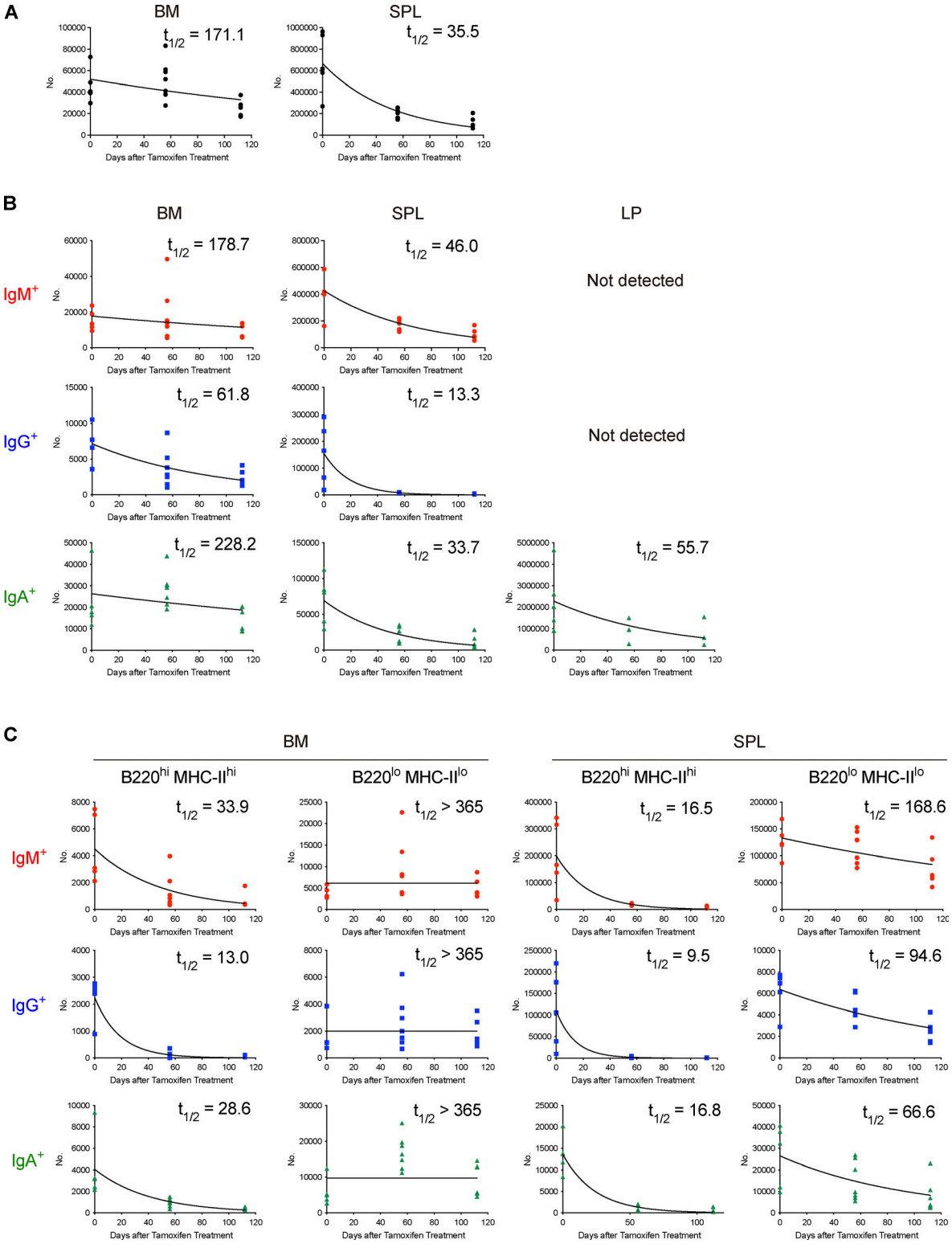

Figure S2. **Half-life of PC populations. (A)** Half-lives ($t_{1/2}$) of tdTomato$^+$ total PCs in BM and SPL calculated from data shown in Fig. 1. Five to seven mice were analyzed at each time point. **(B)** Half-lives ($t_{1/2}$) of IgM$^+$, IgG$^+$, and IgA$^+$ tdTomato$^+$ PCs in BM, SPL, and LP calculated from data shown in Fig. 1. Five to seven mice were analyzed at each time point. **(C)** Half-lives ($t_{1/2}$) of IgM$^+$, IgG$^+$, and IgA$^+$ tdTomato$^+$ PC subsets (B220^{hi} MHC-II^{hi} or B220^{lo} MHC-II^{lo}) in BM and SPL calculated from data shown in Fig. 3. Five to seven mice were analyzed at each time point. Data collected from six independent experiments are combined for calculation of PC half-lives.

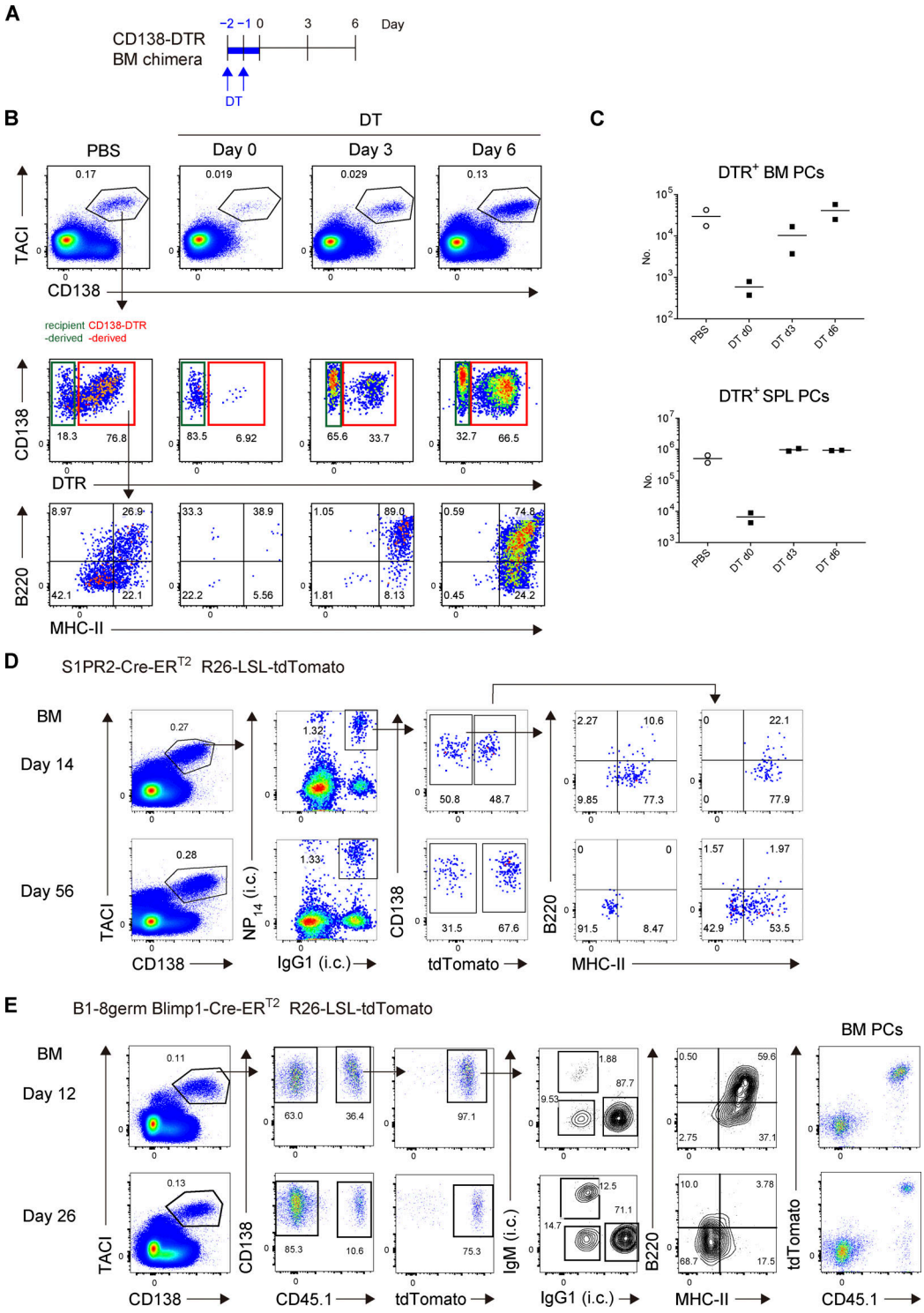

Figure S3. **Gating strategy for identifying de novo–generated homeostatic PCs or NP-specific PCs. (A–C)** Depletion and de novo generation of PCs in CD138-DTR BM chimeric mice. **(A)** Schematic of the experimental procedure. The BM chimeric mice were generated by transfer of BM cells from CD138-DTR mice into x-ray irradiated mice, which were treated with PBS or DT for 2 d. Donor cell-derived PCs in BM, which could be distinguished from residual host-derived PCs by expression of DTR, were analyzed by FCM at the indicated time points. **(B)** Representative FCM data showing expression of DTR by PCs or B220/MHC-II expression by DTR$^+$ PCs at the indicated time points. **(C)** Absolute number of donor-derived PCs in SPL (upper) or BM (lower) at the indicated time points after DT treatment. Two mice were analyzed at each time point. **(D)** Gating strategy for identifying NP-specific PCs in Fig. 4 A. S1pr2-CreER^{T2} R26-LSL-tdTomato mice were immunized with NP-CGG in alum and treated with tamoxifen from days 5 and 6 after immunization. On day 14 and 56, single-cell suspensions were prepared from the BM and stained with cocktails of fluorescent antibodies or an NP probe and analyzed by FCM. Data are representative of two independent experiments. **(E)** Gating strategy for identifying B1-8^{germ} PCs. B6 mice were transferred with splenic B cells from B1-8^{germ} Blimp1-CreER^{T2} R26-LSL-tdTomato mice, immunized with NP-CGG in alum, and then treated with tamoxifen from day 9 to 11 after immunization. BM cells were analyzed by FCM on day 12 and 26. Data are representative of three independent experiments.

Video 1. **Changes of PC dynamics during their maturation, related to** Fig. 5**.** A representative intravital time-lapse imaging (30 min duration, 30 s/time point) of skull bone tissues from the mice at the indicated time points after immunization. Red, PCs expressing tdTomato; green, blood vessels (Qdot); blue, bone tissues (SHG). Scale bar, 20 mm. Data are representative of two independent experiments. Frame rate is 10 frames per second.